NATIONAL AERONAUTICS AND SPACE ADMINISTRATION

Technical Memorandum 33-688

Modal Test of the Viking Orbiter

E. L. Leppert

B. K. Wada
Jet Propulsion Laboratory

R. Miyakawa
Martin Marietta Corporation

JET PROPULSION LABORATORY

CALIFORNIA INSTITUTE OF TECHNOLOGY

PASADENA, CALIFORNIA

July 15, 1974

PREFACE

The work described in this report was performed by the Applied Mechanics Division of the Jet Propulsion Laboratory.

The Jet Propulsion Laboratory is responsible for the Viking Orbiter System, which is part of the overall Viking Project managed by the Viking Project Office at Langley Research Center for NASA.

CONTENTS

PRECEDING PAGE BLANK NOT FILMED

FIGURES

ABSTRACT

A modal test of the Orbiter Development Test Model (ODTM) has been conducted to verify, or update, the mathematical model used for load analysis. The approach used to assure the quality and validity of the experimental data is defined, the modal test is described, and test results are presented and compared with analysis results. Good correlation between the analyses and the test data assures an acceptable model for incorporation into the mathematical model of the launch system.

I. INTRODUCTION

The Jet Propulsion Laboratory is responsible for the Viking Orbiter System (VOS), which is part of the overall Viking Project managed for the National Aeronautics and Space Administration by the Viking Project Office at Langley Research Center. Two Viking spacecraft will be individually launched on a new Titan IIIE/Centaur D-1T launch vehicle in August 1975.

The analysis process used to define design loads utilizes mathematical models of the launch system and of the Viking spacecraft. The information is in the form of modal characteristics and requires the use of modal coupling techniques for solution with present computers (Ref. 1). Experimental verification of the dynamic characteristics is necessary to provide confidence that the analysis model adequately represents the actual structure.

The major objectives of the test (Ref. 2) were to determine the dynamic characteristics and to evaluate the dynamic load paths of the Orbiter Development Test Model (ODTM) configuration. Special efforts were made to ensure that the accelerometer measurements would provide valid dynamic information. Strain gage measurements were desired at the highest feasible excitation level consistent with constraints to limit the accumulation of fatigue damage.

Before the tests reported in this paper were conducted, modal tests had been made on major and minor substructures of the VOS. Some of these tests were conducted to provide improved dynamic predictions for the mathematical model of the modal test configuration. These included tests of the propellant tank ("slosh" test), propulsion module, scan platform, and cable trough. Additional tests were conducted on the solar panels and the high-gain antenna to provide experimentally updated characteristics for inclusion in the final mathematical model of the VOS.

The general techniques described below for obtaining valid data and for data evaluation and correlation for the modal test configuration were also used in the substructure tests. In some cases, improvements were made in the test operation as a result of the substructure test experience. Each test contributed to better definition of the dynamic characteristics of the modal test configuration and thus to improved confidence in the modal test predictions.

The planned approach to assure the quality and validity of the test results included computer programs especially written for pre-test and post-test calculations together with data checks made during the tests. The computer program outputs provided information for conducting the tests, for evaluating and correlating the test results with analysis predictions (Ref. 3), and for delineating the source of differences.

II. MATHEMATICAL SUMMARY

A brief description of the mathematical operations and terminology used in this test is provided below, primarily in the form of definitions. (Complete development can be found in Refs. 3-5.)

$[m]_A$, $[m]_T$ — mass matrix; analytical, test

$[\phi]_A$, $[\phi]_T$ — normalized mode shape matrix (vectors); analytical, test

$[\phi]_R$ — rigid-body vectors

$[\phi]_A^T [m]_T [\phi]_A \overset{?}{=} \lceil m \rfloor$ — test for validity of $[m]_T$ (1)

$[\phi]_T^T [m]_T [\phi]T \overset{?}{=} \lceil m^{ee} \rfloor_T$ — orthogonality, test, elastic-elastic mass matrix   (2)

$[m^{rr}]$ — rigid-body mass matrix

$[m^{er}]$ — rigid-elastic mass coupling

$$\begin{bmatrix} m^{rr} & m^{re} \\ m^{er} & m^{ee} \end{bmatrix}$$ — total elastic and rigid-body matrix

$[m^{re}] [m^{ee}]^{-1} [m^{er}] = \left[m_{eff}^{rr} \right]$ — effective mass   (3)

$[m^{rr}] - [m_{eff}^{rr}] = [m_{res}]$ — residual mass matrix   (4)

$[\phi']_{T,A}$ — analytical modes expressed at accelerometer locations

$$\{\overline{m}\}_T = [\phi']_{T,A} [m]_T \{\phi j\}_T \qquad \text{cross orthogonality check} \qquad (5)$$

$$m_{jJ}^{EE} = \sum_{\ell=1}^{N} \sum_{k=1}^{N} \phi_{ik} M_{k\ell} \phi_{\ell j} \qquad \text{local kinetic energy, where} \qquad (6)$$
$$\phi_{ij} \text{ are velocities}$$

Note that the normalization for the orthogonality matrices is such that each diagonal term is 100%. The effective mass terms for each mode are also presented in terms of percent of the total rigid-body value. Rigid body and rigid-elastic weight matrices are used in place of mass matrices, and residual weight plots result.

III. TEST CONFIGURATION

The configuration selected for the modal test (Fig. 1) included a rigid simulation of the Viking Lander capsule (VLC), the Viking Lander capsule adapter (VLCA), the Viking Orbiter, the Viking spacecraft adapter, and the two adapters connecting the spacecraft to the Centaur booster (the Viking transition adapter (VTA) and the Centaur truss adapter (CTA)). The Viking Orbiter test configuration included the bus, propulsion module, scan platform, and cable trough. Specifically excluded were the solar panels and the high- and low-gain antennas, which had been tested earlier. The thermal blankets were also excluded from the test article.

The rationale for selecting the components of the test configuration included the necessity to verify the analytical interfaces between the test article and both the flexible lander and the Centaur booster, together with the requirement to obtain accurate information on the dynamic characteristics of the major components of the VOS.

The inclusion of the rigid lander and the VTA/CTA trusses verify the mathematical interfaces. The ability to attach shakers and position accelerometers took precedence over inclusion of some less important components.

IV. DETERMINATION OF INERTIAL PROPERTIES

The inertial properties of each item of the test article were experimentally determined or were calculated using measured weights and a

detailed (estimated) weight distribution of the item. In particular, the properties of each bus bay were obtained by using measured values of the contents of the bay, supplemented by calculation of the bus structure contribution. Similar weight calculations were made for other items; the resulting weights were used in both analysis and test prediction and in correlation calculations. Figure 2 defines the node identification used in conjunction with Table 1 to define the node position and inertial properties.

The propellant tanks were filled to the flight ullage condition with referee fluids (liquid Freon and isopropyl alcohol) and pressurized to 6895 N/m^2 (100 psi) above ambient. The "effective" weight parameters were obtained from the results of the "slosh" and propulsion module modal tests.

The total weight of the test article was 3380 kg (7456 lb)[1] of which 1462 kg (3235 lb) (43%) was liquid. The breakdown into weight items was coordinated with accelerometer positions so that the contribution of the significant portion of the structure to the total kinetic energy was correctly accounted for. For each weight item, a transformation for relating the accelerometer readings to the 6 degrees of motion of the lumped mass was generated and was inverted to prove its validity.

Meaningful comparisons between experimental and analytical results (such as orthogonality) are not possible if the inertial properties for each are not realistic and compatible. The difficulty arises in part because the analysis uses a more detailed distribution and generates mode shapes at many structural node points, whereas the experimental distribution uses larger "lumped" masses and measures motion with a limited number of accelerometers. To determine that there was equivalence, a transformation of the analysis mode shapes to accelerometer readings was made and was used with the experimental mass matrix to obtain an "orthogonality" matrix (see Table 2 and Eq. 1). The small magnitude of the off-diagonal terms indicates the validity of the experimental mass distribution.

---

[1] All measurements and calculations were made using U.S. customary units.

V. TEST FACILITY AND INSTRUMENTATION

The test was conducted in a special test facility consisting of a seismic base and a test tower. The test tower provided sets of beams and cranes for pendulous support of electrodynamic shakers, as well as catwalks and ladders for adjusting the cranes and for access to the test article (Figs. 3a, b). The test article was instrumented with 125 accelerometers and 290 strain gages distributed as shown in Table 3. Figures 4a, b, c, d, e show the positioning of the accelerometers on the rigid lander, bus, propulsion subsystem, scan platform and cable trough.

The accelerometer data acquisition system utilized a scanner to acquire the acceleration signals sequentially in a preselected order. The output of each scanned accelerometer signal and of a reference accelerometer signal (selected for each mode) was fed through matched tracking filters to a gain-phase meter, where it was reduced to ratio and phase angle form and converted by a coupler and teletypewriter to printed and punched tape output. The strain gage system acquired data in a similar manner.

Provision was made for inserting tracking filters with wider bandwidths for the higher-frequency resonances, thus allowing the scanner to operate at an increased rate and to reduce the data acquisition time. Information to fully identify each run was manually inserted with the teletypewriter.

Figures 5a and 5b are block diagrams of the two systems. Note that provision was made for patching the outputs of the strain gage system through the accelerometer systems in case of failure of a critical component. The equipment could operate in a "manual select" mode to allow examination of acceleration ratio and phase of any individual channel.

VI. TEST OPERATIONS

The test article was excited by (up to) ten 111-N (25-lb) peak force Ling shakers. The system provided separate power supplies for the field and armature current; an oscillator to control the frequency of excitation; meters, oscillographs, and oscilloscopes to monitor the operation; and a means to

simultaneously open the armature circuits for decay measurement to evaluate damping. Provision was made for exciting the major weight items of the system in three orthogonal axes (Figs. 6a, b, c) and for rotational excitation of the bus and of the rigid lander. For high-frequency modes, which showed motion primarily on such items as the cable trough and the propellant tank (both of which were effectively "hidden" by the rigid lander and the bus), excitation was limited to shakers attached to the bus and to the scan platform.

The physical operations used to find and isolate the "pure" modes of the test article followed a normal pattern of searching for a response peak, then adjusting shaker positions, forces, and phases until Lissajou figures of force and velocity closed. For a simple system with good frequency separation and little stiffness or inertia coupling, this is an adequate approach. Initial calculations of the dynamic characteristics of the test article indicated that this approach would probably not be completely adequate. To supplement the approach, computer programs were formulated to provide tables of predicted frequencies as well as mode shapes in the form of normalized accelerometer readings, normal mode plots (see appendix), and plots of residual weight.

Figures 7a-f are examples of residual weight plots (Refs. 4, 5). The plots measure the importance of the mode in each of the six directions and the number of modes remaining to be isolated. In conjunction with the typical plots of mode shapes (Figs. 8a, b, c) and tables of kinetic energy distribution (Table 4), the residual weight plots provided information for placement, phase, and force levels required to excite each mode. The tabulated mode shape data, used for calculation of Table 2, allowed selection of the reference accelerometer channel and, with the data acquisition system in the "manual mode," a means for checking the amplitude and phase readings of important accelerometers with the predicted values. If these comparisons were not satisfactory, additional adjustments of frequency and shakers were made.

When satisfactory isolation was obtained, the accelerometers and strain gages were recorded and oscillograph decay records of selected accelerometers obtained. Additional recordings of each mode were obtained at higher levels, with adjustment of frequency and shaker force, if required, to reestablish the mode. These tests were made to obtain damping at high levels and to establish the linearity characteristics of the test article.

As each recording was completed, the punched paper tapes were transmitted to storage in an 1108 computer and were processed by special data reduction and evaluation programs.

The oscillograph decay records were processed by measuring the "double" amplitude of the decaying traces as shown by Fig. 9, with selection of the number of cycles between readings determined by the analyst. A simple computer program processed the data (Table 5) to determine the damping coefficient $2 \ c/c_{cr}$.

The decay traces were not filtered, since filters can alter the decay rate. Only the high-amplitude accelerometer channels were recorded to ensure traces as "clean" as possible.

After all the excitable modes for a given direction were obtained, sine sweeps were made to reveal possible additional modes. Routinely, a mode obtained early in a given shaker setup was reacquired before the setup was changed. The information provided a verification that the data acquisition system did not change during the test. In several cases, a mode was excited a second time by shakers in a different basic force direction.

VII. DATA CHECKS

Prior to and during the test operation, planned checks were made to ensure that good strain gage and accelerometer data would be acquired. Additional checks were instituted as a result of anomalies encountered during the test.

During assembly and disassembly of the test article, and before and after each test period, static strains were recorded, processed, and compared with predicted values. Before and after each test period, a scan of excitation voltage was taken. Good comparison of these readings to a standard set indicated that the data were valid. Any significant change was investigated to determine the cause of the discrepancy. A similar check on the gain-phase meter output was included when an intermittent error in output numbers was observed.

The dynamic strain gage records were processed to define the stresses and loads applied to each of the significant members during excitation of each

mode. Allowable stresses and loads, defined to limit fatigue damage in the member, were stored and compared to actual loads (or stresses) to obtain an allowable ratio of increased excitation. Table 6 is an excerpt from the printout for mode 701E.

The accelerometer data were checked by comparisons between original and reacquired modes, by routine on-line comparison of modes at successively higher levels of excitation, and by listing the accelerometers having a consistently low output. A major accelerometer data error, caused by base sensitivity to stress (transmitted through a 3.18 cm (1.25-in.) micarta block), was detected by observing a distorted mode shape (Fig. 10).

VIII. RESULTS AND DISCUSSION

The total number of measured modes is tabulated in Tables 7 and 8. The columns list modes in increasing levels of response. As planned, all the important structural modes below 30 Hz were obtained, many at multiple levels of excitations. An initial set of data was at least partially invalidated by problems in strain gage readout or erroneous accelerometer readings, but adequate checks were developed to ensure the validity of the final measurements.

In several cases, the same basic mode was excited from different shaker positions. Consequently, two identifying numbers have been assigned (as for the 19.61- and 19.82-Hz modes). Only mode numbers with 7 as a leading digit are good in all respects.

The most usually accepted measure of good modal data is the orthogonality of the modes as defined by Eq. (2). The pretest criterion goal for off-diagonal terms was 10% or less. From Table 9, the maximum term is 6.2%, with only three terms equal to or greater than 5%.

The high-frequency modes listed in Table 8 were excited by shakers attached at the bus and at the scan platform and include modes having mostly "local" motion. Table 10 shows orthogonality values for modes in this group; Table 11 show orthogonality with respect to the low-frequency group. The

considerable increase in some off-diagonal terms reflects the difficulty in exciting "pure" modes when only local high-frequency modes remain and the excitation forces cannot be favorably placed.

Since the motion of the experimental mode is defined by a limited number of accelerometer positions, the mass matrix used cannot be considered exact. However, the orthogonality matrix of Table 2 indicates that an adequate representation has been used for the major modes.

The experimental frequencies show good comparison with the analytical predictions (except for one mode), with an average increase of about 5.5% over the analytical (Table 12). Typical correspondence of the modes is shown by means of the effective mass (Table 13) and by modal plots (Figs. 8 and 11). In each case, the relationship between analytical and experimental data is good. Table 13 verifies that the major modes have been obtained when a minimum of 89% of the effective mass is accounted for.

Additional examples of good comparisons are found in "cross correlation" (Table 14) of 30 analytical modes with experimental mode 701. Perfect correlations would show a value of 1.0 with analytical mode 3 and zero with all others. A summary is shown in Table 15. Similarly good comparison between analytical and experimental data is shown by comparisons of the local kinetic energies (Tables 4 and 16). Additional comparison of modes shapes is shown in Ref. 3.

Although good comparison of the analytical and experimental results does not necessarily assure that the experimental data are good, when an analysis is updated by data obtained from modal tests of substructures, a good comparison tends to reinforce the validity of both.

The accuracy of modal strain is more difficult to establish. One representative mode is presented to help establish the accuracy as related to data scatter on strain magnitude. Figure 12 shows small scatter over a stress range approaching specified stress limits. (Since the limits were set to preclude possibility of fatigue damage, the member loads and strains are not large.)

Other methods were used to establish strain gage accuracy. The modal forces can be evaluated from strain gage or by a static solution of a structure

by applying modal inertial forces. Table 17 shows the Viking Lander capsule adapter results compared on this basis. Table 18 shows the Viking spacecraft adapter results based on the reactive forces from the VTA into the struts. A general observation is that the strain gage readings are accurate to within 25% if the magnitude of the strain is greater than 5 μcm/cm (μin./in.).

Damping was generally low, with the highest value of 2% critical corresponding to the two lowest frequencies. From Table 19, the lowest value was 0.4% critical for a mode which was dominantly rigid lander rotation about the Y axis.

In general, the structure responded in a linear manner for the level of excitation achieved, as shown by the strain curves. Figure 13 shows a characteristic reduction of frequency with increased response; however, the percentage reduction is small. Figure 14 shows characteristic responses of peak acceleration vs shaker force, with good linearity in the low response levels and a reduction in response at the higher force levels. Figure 15 shows a trend toward increased damping with increased excitation for the 7.8-Hz mode.

IX. SUMMARY AND CONCLUSIONS

A modal test has been conducted on the ODTM configuration of the Viking spacecraft using a coordinated approach of analysis and test. Results from modal tests of substructures, conducted earlier, were used to provide data to improve the analytic model of the test article, from which high-confidence predictions of test characteristics were obtained.

The good correlation that was obtained between analyses and post-test data reductions reinforces the validity of both types of data and assures an acceptable model for incorporation into the dynamic analysis to obtain anticipated flight member loads.

REFERENCES

1. Wada, B. K., "Viking Orbiter Dynamics," presented at the 44th Shock and Vibration Symposium, held at Houston, Texas, Dec. 4-7, 1973, sponsored by the Shock and Vibration Information Center, Washington, D. C.

2. Leppert, E., VO'75 Test Plan, ODTM with VTA/CTA Modal Test, JPL internal document PD 611-59, Jet Propulsion Laboratory, Pasadena, California, May 9, 1973.

3. Wada, B. K., Garba, J., and Chen, J., "Development and Correlation, Viking Orbiter Analytical Dynamic Model With Modal Test," presented at the 44th Shock and Vibration Symposium, held at Houston, Texas, Dec. 4-7, 1973, sponsored by the Shock and Vibration Information Center, Washington, D. C.

4. Bamford, R. M., Wada, B. K., and Gayman, W. H., Equivalent Spring-Mass System for Normal Modes, Technical Memorandum 33-380, Jet Propulsion Laboratory, Pasadena, California, Feb. 15, 1971.

5. Wada, B. K., Bamford, R., and Garba, J., "Equivalent Spring Mass: A Physical Interpretation," Shock and Vibration Bulletin 42, Jan. 1972.

Table 1a. Coordinate locations and inertial data (SI units)

Node		Coordinate location[a] X	Y (m)	Z	Weight, kg W_x	W_y	W_z	Inertia kg-cm^2 I_{xx}	I_{yy}	I_{zz}
1	Spacecraft bus	1.192	-0.0046	0.2466	27.7	27.7	27.7	8585	6390	5555
2	Spacecraft bus	0.9847	0.3894	0.2322	30.2	30.2	30.2	12068	10730	9615
3	Spacecraft bus	0.6533	0.6698	0.2268	27.1			11360	9618	8234
4	Spacecraft bus	0.3967	1.0315	0.2210	22.2			6390	4844	3366
5	Spacecraft bus	-0.0261	1.1918	0.2609	31.2			11942	7680	6378
6	Spacecraft bus	-0.3594	0.9977	0.2266	27.9			7628	10900	6065
7	Spacecraft bus	-0.8827	0.8433	0.3393	23.2			18458	24525	15604
8	Spacecraft bus	-0.9436	0.4026	0.2596	19.5			6808	7297	6428
9	Spacecraft bus	-1.2377	0.0005	0.2327	40.4			9882	4721	5950
10	Spacecraft bus	-0.9977	-0.4234	0.2316	27.0			11945	8207	9767
11	Spacecraft bus	-0.6896	-0.6767	0.2273	27.0			11556	9363	8219
12	Spacecraft bus	-0.4267	-1.0300	0.2654	36.6			13757	12127	6451
13	Spacecraft bus	0.0091	-1.1763	0.2342	40.3			9981	4704	5886
14	Spacecraft bus	0.3990	-1.0226	0.2223	22.2			4917	6187	3413
15	Spacecraft bus	0.7183	-0.6782	0.2370	24.2			7654	8477	5801
16	Spacecraft bus	0.9947	-0.4138	0.2062	33.0			10294	13426	11108
101	Lander	00	00	1.9891	1164			612 +4	651 +4	1012 +4
301	Oxidizer tank	0.4661	00	0.7887	815	815	1011	416 +3	416 +3	107 +3
303	Fuel tank	-0.4661	00	0.7287	494	494	568	295 +3	313 +3	98 +3
401	Pressure tank	00	-0.0008	0.2715	36.5	36.5	36.5	24415	24525	24415
501	Thrust point	0.0048	-0.0348	-1.5304	25	25	25	12381	6586	14928
201	Scan platform	-0.8547	0.9929	0.4712	83	83	83	1914 +2	1678 +2	1417 +2
402	PCA[b]	0.2438	-0.4877	-0.2662	4.1	4.1	4.1	-	-	-
403	PCA[b]	-0.0025	-0.4877	-0.2662	4.5	4.5	4.5	-	-	-
404	PCA[b]	-0.2413	-0.4877	-0.2662	4.1	4.1	4.1	-	-	-
601	Cable trough	00	0.7262	0.4064	5.7	5.7	5.7	-	-	-
602	Cable trough	-0.7262	00	0.4064	5.7	5.7	5.7	-	-	-
603	Cable trough	00	-0.7262	0.4064	5.7	5.7	5.7	-	-	-
604	Cable trough	0.7262	00	0.4064	5.7	5.7	5.7	-	-	-

[a]Spacecraft coordinates.

[b]Pressure control assembly.

Table 1b. Coordinate locations and inertial data (English units)

Node		Coordinate location[a] X	Y (in.)	Z	W_x	Inertia data W_y (lb)	W_z	I_{xx}	I_{yy} lb-in.^{2}	I_{zz}
1	Spacecraft bus	46.93	-0.18	9.71	61.096	61.096	61.096	2933	2183	1898
2	Spacecraft bus	38.77	15.33	9.14	66.701	66.701	66.701	4123	3666	3285
3	Spacecraft bus	25.72	26.37	8.93	59.659	59.659	59.659	3881	3286	2813
4	Spacecraft bus	15.62	40.61	8.70	48.927	48.927	48.927	2183	1655	1150
5	Spacecraft bus	-1.03	46.92	10.27	68.661	68.661	68.661	4080	2624	2179
6	Spacecraft bus	-14.15	39.28	8.92	61.388	61.388	61.388	2606	3724	2072
7	Spacecraft bus	-34.75	33.20	13.36	51.165	51.165	51.165	6306	8379	5331
8	Spacecraft bus	-38.15	15.85	10.22	43.004	43.004	43.004	2326	2493	2196
9	Spacecraft bus	-48.73	0.02	9.16	88.986	88.986	88.986	3376	1613	2033
10	Spacecraft bus	-39.28	-16.67	9.12	59.6	59.6	59.6	4081	2804	3337
11	Spacecraft bus	-27.15	-26.64	8.95	59.4	59.4	59.4	3948	3199	2808
12	Spacecraft bus	-16.80	-40.55	10.45	80.727	80.727	80.727	4700	4143	2204
13	Spacecraft bus	0.36	-46.31	9.22	88.946	88.946	88.946	3410	1607	2011
14	Spacecraft bus	15.71	-40.26	8.75	48.943	48.943	48.943	1680	2114	1166
15	Spacecraft bus	28.28	-26.70	9.33	53.39	53.39	53.39	2615	2896	1982
16	Spacecraft bus	39.16	-16.29	8.12	72.609	72.609	72.609	3517	4587	3795
101	Lander	0.00	0.00	78.31	2567	2567	2567	2091513	2223887	3458324
301	Oxidizer tank	18.35	0.00	-31.05	1797.4	1797.4	2229.1	142209	142209	36487
303	Fuel tank	-18.35	0.00	-28.09	1088.425	1088.425	1252.13	100770.6	10689.3	33525
401	Pressure tank	0.00	-0.03	10.69	80.53	80.53	80.53	8341.6	8378.7	8341.6
501	Thrust point	0.19	-1.37	-60.25	55.0	55.0	55.0	4230	2250	5100
201	Scan platform	-33.65	39.09	18.55	183.0	183.0	183.0	65410	39890	48400
402	PCA[b]	9.60	-19.20	-10.48	9.0	9.0	9.0	-	-	-
403	PCA[b]	-0.10	-19.20	-10.48	9.85	9.85	9.85	-	-	-
404	PCA[b]	-9.50	-19.20	-10.48	9.0	9.0	9.0	-	-	-
601	Cable trough	0.00	28.59	16.00	12.475	12.475	12.475	-	-	-
602	Cable trough	-28.59	0.00	16.00	12.475	12.475	12.475	-	-	-
603	Cable trough	0.00	-28.59	16.00	12.475	12.475	12.475	-	-	-
604	Cable trough	28.59	0.00	16.00	12.475	12.475	12.475	-	-	-

[a]Spacecraft coordinates.

[b]Pressure control assembly.

Table 2. Orthogonality of analytical modes and test mass matrix[a]

4.35	4.40	7.48	7.83	10.92	13.36	14.64	17.95	18.81	23.42	24.28	26.18	Frequency, Hz
1	2	3	4	5	6	7	8	9	10	11	12	Mode
100	0.9	-0.3	-0.2	0.8	-0.9	1.4	1.6	-1.7	-0.3	-0.9	0.4	1
	100	-0.2	-0.2	0.3	0.1	-0.1	0.2	-3.1	0.4	-2.2	-0.4	2
		100	1.3	-1.6	1.1	-1.7	-1.4	0	-2.1	-1.2	0.7	3
			100	-0.4	1.2	-0.2	-0.3	-2.7	1.7	-0.3	1.1	4
				100	1.0	0.8	1.1	-0.6	2.2	-0.2	1.1	5
					100	0.4	-0.7	0.8	0.9	-0.9	1.8	6
						100	-1.8	0	0.2	-2.3	0.9	7
							100	-0.2	-1.4	1.2	-0.2	8
								100	-0.9	0.7	-1.4	9
									100	-1.0	0.2	10
										100	-2.3	11
											100	12

[a]See Eq. (1).

Table 3. Instrumentation distribution

Substructure	Accelerometers	Strain gages
Rigid lander	6	
VLCA		18
Bus (16 bays)	72	163
Cable trough	8	
Scan platform	6	
Attitude control support		4
Viking spacecraft adapter		36
Propulsion module	33	69
Total	125	290

Table 4. Analytical local kinetic energy (analysis mode 701)[a]

Node	Local kinetic energy distribution, %						
	X	Y	Z	θ_x	θ_y	θ_z	Sum
1	0.08	0.31	0.00	0.00	0.00	0.00	0.40
2	0.20	0.06	0.00	0.00	0.00	0.00	0.26
3	0.05	0.05	0.00	0.00	0.00	0.00	0.11
4	0.00	0.06	0.00	0.00	0.00	0.00	0.06
5	0.01	0.10	0.02	0.00	0.01	0.00	0.13
6	0.01	0.11	0.01	0.00	0.00	0.00	0.14
7	0.06	0.13	0.00	0.00	0.00	0.00	0.19
8	0.16	0.08	0.00	0.00	0.00	0.00	0.24
9	0.09	0.66	0.01	0.00	0.00	0.00	0.77
10	0.02	0.50	0.02	0.00	0.00	0.00	0.54
11	0.01	0.51	0.01	0.01	0.01	0.00	0.55
12	0.16	0.84	0.03	0.00	0.00	0.00	1.03
13	0.00	1.02	0.02	0.00	0.00	0.00	1.05
14	0.12	0.35	0.00	0.00	0.00	0.00	0.48
15	0.02	0.39	0.00	0.00	0.00	0.00	0.41
16	0.00	0.51	0.00	0.00	0.00	0.01	0.53
101	5.39	3.98	0.01	0.43	7.59	62.20	79.61
301	4.55	3.60	0.03	0.02	0.00	0.11	8.32
303	2.63	0.33	0.01	0.02	0.02	0.10	3.10
401	0.14	0.00	0.00	0.00	0.00	0.03	0.18
501	0.19	0.04	0.00	0.00	0.00	0.02	0.25
201	0.95	0.06	0.07	-0.02	0.24	-0.03	1.27
402	0.05	0.00	0.00				0.05
403	0.05	0.00	0.00				0.05
404	0.05	0.00	0.00				0.05
601	0.02	0.01	0.00				0.03
602	0.02	0.10	0.00				0.12
603	0.01	0.00	0.00				0.01
604	0.01	0.07	0.00				0.07
	15.02	13.89	0.26	0.46	7.90	62.46	100.01

[a]Frequency = 7.48 Hz.

Table 5. Damping data reduction

```
***********************************   ***  *******  ***********

        MODAL DECAY REDUCTION
GAMMA=2C/C(CRITICAL)


  MODE NUMBER  712 FIRST RUN
FREQ=19.82 HZ

  NUMBER OF CYCLES BETWEEN READINGS   10
  DECAYS FOR    ACCEL. NO.   75
```

INCREMENT	AMPLITUDE	RATIO	GAMMA
1	90	0	0
2	70.5	.783333	7.773037E-3
3	52.2	.740426	9.566182E-3
4	37.4	.716475	.010613
5	·27.8	.743316	9.442183E-3
6	22.5	.809355	6.732918E-3
7	20	.888889	3.749154E-3
8	16.2	.81	6.707464E-3
9	13	.802469	7.004793E-3
10	10.5	.807692	6.79828E-3
11	9	.857143	4.906773E-3

```
  AVERAGE DECAY CONST FOR THIS DECAY =  7.329362E-3

  DECAYS  FOR ACCEL. NO.   111
```

INCREMENT	AMPLITUDE	RATIO	GAMMA
1	101	0	0
2	69	.683168	.012128
3	54.2	.785507	7.684822E-3
4	45.5	.839483	5.569427E-3
5	35	.769231	8.351321E-3
6	26.9	.768571	8.378616E-3
7	21	.780669	7.851482E-3
8	17	.809524	6.726183E-3
9	15.5	.911765	2.940336E-3
10	12.2	.787097	7.620475E-3
11	10.8	.885246	3.879877E-3

```
  AVERAGE DECAY CONST FOR THIS DECAY =  7.11606E-3

THE OVERALL AVERAGE DECAY CONSTANT FOR BOTH DECAYS= 7.222711E-3

   ****************************   *********  ****  *********
```

Table 6. Strain gage data reduction, mode 701E[a, b]

Member	Allowable force, N	Actual force, N	Allowable stress, N/m^2	Actual stress, N/m^2
750	2491	20		
751	2491	-1666		
752	2491	979		
753	2491	-1933		
754	2491	2329		
755	2491	509		
686	11, 565	129		
687	11, 565	743		
688	11, 565	2158		
689	11, 565	-1219		
690	11, 565	-680		
691	11, 565	14		
692	11, 565	-550		
693	11, 565	131		
694	11, 565	680		
695	11, 565	-1685		
696	11, 565	-183		
697	11, 565	715		
806	26, 688	273		
810	6227	1718		
811	5782	80		
813	6227	-185		
816	26, 688	-1589		
818	26, 688	-1790		
820	6227	66		
B2-821			184, 475	-751
B3-821			184, 475	-3023
823	6227	-230		
826	26, 688	2204		

Table 6 (contd)

Member	Allowable force, N	Actual force, N	Allowable stress, N/m^2	Actual stress, N/m^2
830	6227	-1		
831	5782	-451		
832	6227	580		
835	26,685	-988		
839	6227	-855		
840	5782	150		
841	6227	-265		
B1-877			184,475	1136
B2-877			184,475	-563
B1-883			184,475	-786
B2-883			184,475	224
A1-250			184,475	2603

[a]Allowable force ratio = 1.0692

[b]Allowable stress ratio = 9.4513

Table 7. Summary of measured modes

Modes	708	743	701	702	704	705	711	709	712	707	713	714
Freq Hz	4.51	4.65	7.84	8.30	11.51	14.19	15.35	19.61	19.82	24.85	26.49	29.54
First Modes	008	003	001	002	004	005	010	017	006	007	013	014
	108	103	101	102	004R[a]	105	011	217	106		113	114
	208	203	201	202	104	205	111		206		213	
		303	301		204	005R	211		012		113R	
			401		304R	305	111R		112		213R	
			601				211R		212			
"Good" Modes	708	703	701	702	704	705	711	717	706	707	713	714
	708[b]	703R	701[b]	732[b]	704R	705R	711[b]	709	712	737	713[b]	714[b]
		733	701A[c]		704[b]	705[b]		709[b]	712R	747		
		743	701B[c]						712[b]			
		753	701C[c]									
		753[b]	701D[c]									
			701E[c]									

[a] Repeat.

[b] High level runs (all data are not recorded).

[c] Limited subset of strain gages.

Table 8. Summary of high-frequency measured modes

Frequency, Hz											
32.22	32.73	34.24	34.89	35.36	40.18	43.84	47.6	49.29	34.18	29.59	84.70
721	720	728	722	718	719	716	723	715	803	801	802
721[a]	720[a]		722[a]	718[a]	719[a]	716[a]	723[a]	715[a]	813[a]	811[a]	812[a]

[a]High-level run (not all data taken).

Table 9. Orthogonality of test modes[a]

4.51	4.65	7.84	8.30	11.51	14.19	15.35	19.61	19.82	24.85	26.49	29.34	Frequency, Hz
708	743	701	702	704	705	711	709	712	707	713	714	Mode
100	6.2	-0.2	-1.1	-0.3	1.1	-2.3	-1.9	-1.7	0.6	0	-0.6	708
	100	0.1	-1.2	-4.1	3.0	-0.9	-2.4	1.0	-1.2	-1.5	-2.5	743
		100	0.4	0.8	1.6	-0.2	-0.7	-1.5	-0.5	0.4	3.5	701
			100	1.0	1.3	1.2	1.1	-1.8	1.2	-0.5	-0.1	702
				100	0.6	0.8	1.7	-1.0	0.2	-0.4	4.6	704
					100	0.4	-0.6	1.5	4.4	1.6	-5.0	705
						100	-0.1	-0.1	3.6	-1.3	-0.2	711
							100	-2.7	1.0	2.5	-0.2	709
								100	5.9	2.7	-1.1	712
									100	-3.4	-1.9	707
										100	-1.5	713
											100	714

[a]See Eq. (2).

Table 10. Orthogonality for high-frequency modes

32.22	32.73	34.24	34.89	35.36	40.18	43.84	47.6	49.29	Frequency, Hz
721	720	728	722	718	719	716	723	715	Mode
100	29.14	40.34	33.84	22.49	3.13	21.36	5.86	4.31	721
	100	68.67	75.36	76.65	-18.52	5.02	-18.84	24.80	720
		100	97.43	85.41	-26.02	25.25	-4.20	2.04	728
			100	90.99	-32.23	29.63	-3.40	0.52	722
				100	-34.28	11.06	4.55	-2.28	718
					100	-11.72	-2.97	45.09	719
						100	17.92	-6.00	716
							100	-20.17	723
								100	715

24

Table 11. Orthogonality of high-frequency modes with low-frequency modes

32.22	32.73	34.24	34.89	35.36	40.18	43.84	47.6	49.29	Frequency, Hz
721	720	728	722	718	719	716	723	715	Mode
-9.13	0.74	-2.53	-2.53	-9.66	-3.60	-0.73	-7.87	-0.54	708
9.81	2.06	-0.38	-0.61	8.73	4.88	0.11	10.67	-0.80	743
-6.09	1.30	0.35	-0.48	-5.58	-3.33	1.52	-5.50	-1.34	701
3.50	5.63	-0.11	-0.43	2.31	5.97	-0.01	1.57	1.88	702
9.72	2.67	3.07	1.02	7.30	6.92	3.02	5.42	0.23	704
2.89	-1.96	-1.74	1.69	6.56	-0.18	-4.67	5.41	1.78	705
2.42	-0.60	-0.64	-1.66	5.08	2.57	0.05	0.95	0.50	711
3.09	-0.22	4.48	5.22	6.50	1.79	-0.07	-1.92	-0.28	709
3.66	-5.95	-4.11	-2.46	2.42	1.70	-0.86	1.02	-0.64	712
14.78	-0.97	-1.17	-1.23	4.70	1.32	0.33	5.25	-2.15	707
-14.48	15.86	-8.43	-9.43	1.30	-1.69	-1.50	3.57	-0.77	713
51.8	25.09	25.49	21.03	2.85	-0.05	6.52	-1.58	-6.60	714

Table 12. Analysis prediction and modal test frequencies

Analysis mode	Analysis frequency, Hz	Test mode	Test frequency, Hz	Percent deviation
1	4.35	708	4.51	3.55
2	4.40	743	4.65	5.38
3	7.48	701	7.84	4.60
4	7.83	702	8.30	5.65
5	10.92	704	11.51	5.12
6	13.37	705	14.19	5.85
7	14.64	711	15.35	4.63
8	17.96	709	19.61	8.45
9	18.82	712	19.82	5.10
10	23.44	707	24.85	5.75
11	24.28	714	26.49	8.3
12	26.18	713	29.54	11.4

Table 13. Analytical and experimental effective mass in percent[a]

Mode	X	Y	Z	θ_x	θ_y	θ_z
1	96.42[b] (89.51)[c]	1.76 (7.97)	0.01 (0.03)	1.34 (6.12)	85.20 (78.23)	0.14 (0.88)
2	1.67 (3.30)	87.47 (86.49)	0.0 (0.03)	63.66 (64.45)	1.49 (3.15)	1.09 (1.13)
3	0.95 (0.89)	0.28 (0.35)	0.0 (0.01)	1.75 (1.88)	0.02 (0.02)	55.21 (56.91)
4	0.06 (0.10)	5.60 (4.81)	0.03 (0.10)	28.95 (27.51)	0.01 (0.0)	1.94 (1.66)
5	0.05 (0.0)	0.06 (0.11)	0.56 (0.58)	0.10 (0.19)	6.40 (7.80)	19.58 (20.43)
6	0.20 (0.38)	0.06 (0.01)	5.63 (6.67)	0.10 (0.01)	4.77 (5.65)	9.83 (7.39)
7	0.0 (0.01)	0.01 (0.0)	49.02 (51.80)	0.01 (0.0)	0.40 (0.63)	0.25 (0.24)
8	0.02 (0.02)	0.01 (0.0)	12.98 (12.52)	0.01 (0.01)	0.04 (0.0)	0.07 (0.15)
9	0.0 (0.0)	0.06 (0.05)	0.45 (0.90)	0.06 (0.02)	0.0 (0.0)	0.41 (0.09)
10	0.0 (0.0)	0.02 (0.01)	3.15 (0.58)	0.03 (0.03)	0.0 (0.01)	0.0 (0.04)
11	0.0 (0.0)	0.02 (0.01)	13.60 (11.57)	0.07 (0.02)	0.0 (0.0)	0.23 (0.06)
12	0.0 (0.0)	0.02 (0.07)	5.02 (22.17)	0.06 (0.20)	0.0 (0.0)	0.0 (0.06)
Total	99.37 (94.39)	95.37 (100.24)	90.45 (95.96)	96.12 (100.20)	98.33 (95.89)	88.75 (89.15)

[a]See Eq. (3).

[b]Analysis.

[c]Test.

Table 14. Cross orthogonality: orthogonality of test mode 701; run name
DTA701 at frequency 7.84 Hz with respect to all analytical modes

Analytical mode	Frequency, Hz	Orthogonality
1	4.35	-0.001
2	4.40	-0.005
3	7.48	-0.997
4	7.83	-0.015
5	10.92	-0.003
6	13.36	-0.015
7	14.64	0.006
8	17.95	0.023
9	18.81	0.000
10	23.42	0.006
11	24.28	0.011
12	26.18	-0.008
13	28.72	0.001
14	29.98	0.001
15	31.36	-0.020
16	33.54	-0.009
17	34.68	0.004
18	35.80	-0.000
19	36.95	0.011
20	38.43	0.002
21	39.11	-0.088
22	40.58	-0.051
23	42.05	-0.015
24	43.15	-0.003
25	45.32	-0.004
26	45.80	-0.011
27	51.80	0.003
28	52.40	-0.007
29	53.15	0.008
30	59.44	-0.010

Analytical mode 3 has best correlation with test
mode DTA 701 at frequency 7.48 Hz.

Table 15. Correlation summary

Analytical mode	Experimental mode	Analytical frequency, Hz	Experimental frequency, Hz	Cross orthogonality	RSS[a] error
1	708	4.35	4.51	0.903	0.32
2	703	4.40	4.63	0.948	0.24
2	743	4.40	4.65	0.922	0.31
3	701	7.48	7.84	0.997	0.15
4	702	7.83	8.30	0.998	0.13
5	704	10.92	11.51	0.995	0.18
6	705	13.36	14.09	0.992	0.15
7	711	14.64	15.35	0.995	0.16
8	709	17.95	19.61	0.861	0.28
8	717	17.95	19.49	0.918	0.23
9	712	18.81	19.83	0.853	0.57
10	707	23.42	24.85	0.954	0.27
11	713	24.28	26.49	0.779	0.24
12	714	26.18	29.54	0.796	0.51
14	720	29.98	32.73	0.586	0.27
14	722	29.98	34.89	0.762	0.29
14	718	29.98	35.36	0.774	0.28
14	728	29.98	34.24	0.721	0.28
15	721	31.36	32.2Z	0.637	0.48
16	813	33.54	33.43	0.820	0.30
17	719	34.68	40.18	0.677	0.13
19	716	36.95	43.84	0.896	0.24
24	715	43.15	49.29	0.806	0.40
24	723	43.15	47.60	0.478	0.33

[a]Reference 3, page 22, Eq. (37b).

Table 16. Experimental local kinetic energy[a]

Node[b]	Local kinetic energy distribution, %						
	X	Y	Z	θ_x	θ_y	θ_z	Sum
1	0.09	0.27	0.00	0.00	0.00	0.00	0.36
2	0.21	0.05	0.00	0.00	0.00	0.00	0.26
3	0.05	0.03	0.00	0.00	0.00	0.01	0.09
4	0.00	0.05	0.00	0.00	0.00	0.00	0.05
5	0.01	0.08	0.01	0.00	0.00	0.00	0.10
6	0.01	0.07	0.01	0.00	0.00	0.01	0.09
7	0.08	0.14	0.01	0.00	0.01	0.01	0.26
8	0.14	0.06	0.00	0.00	0.00	0.01	0.21
9	0.08	0.62	0.01	0.00	0.00	0.00	0.71
10	0.02	0.54	0.00	0.00	0.00	0.00	0.56
11	0.01	0.42	0.00	0.00	0.0	0.00	0.45
12	0.11	0.84	0.01	0.00	0.06	0.05	1.07
13	0.00	0.84	0.01	0.00	0.00	0.01	0.87
14	0.11	0.24	0.00	0.00	0.00	0.00	0.36
15	0.02	0.31	0.00	0.00	0.00	0.01	0.34
16	0.00	0.45	0.00	0.00	0.00	0.00	0.46
101	4.75	4.03	0.02	0.40	6.56	64.90	80.65
301	4.10	3.51	0.01	0.02	0.00	0.11	7.75
303	2.34	0.43	0.02	0.01	0.03	0.10	2.93
401	0.12	0.00	0.00	0.00	0.00	0.03	0.16
501	0.18	0.04	0.00	0.00	0.00	0.02	0.25
201	0.78	0.10	0.03	0.02	0.60	0.09	1.63
402	0.05	0.00	0.00				0.05
403	0.07	0.00	0.00				0.07
404	0.05	0.00	0.00				0.05
601	0.01	0.01	0.00				0.02
602	0.02	0.09	0.00				0.12
603	0.00	0.00	0.00				0.00
604	0.01	0.06	0.00				0.06
	13.41	13.30	0.15	0.46	7.30	65.38	100

[a] Mode 701; frequency 7.84 Hz.

[b] Nodes:
- 1-16 = bus
- 101 = lander
- 301 = oxidizer tank
- 303 = fuel tank
- 401 = pressurant tank
- 501 = thrust assembly
- 201 = scan platform
- 402-404 = pressure control assembly
- 601-604 = cable trough

Table 17. Viking lander capsule adapter forces

| Member number | Forces,[a] N (lb) | | Percent error |
	Strain gage	Inertial load	
750	716 (161)	779 (175)	8.70
751	236 (53)	209 (47)	11.30
752	1165 (262)	1330 (299)	14.20
753	1240 (279)	1295 (291)	4.20
754	515 (116)	582 (131)	12.80
755	463 (104)	578 (130)	24.60

[a]For mode 713, frequency = 26.49 Hz.

Table 18. Viking spacecraft adapter base reactions

Mode	Force, N			Moment, N - m		
	F_x	F_y	F_z	M_x	M_y	M_z
708	1780[a] (2300)[b]	-535 (-753)	-36 (+240)	1888 (1760)	6790 (5920)	-144 (-177)
703	334 (347)	1710 (1740)	36 (-455)	-5920 (-3820)	1316 (770)	158 (218)
701	200 (222)	-125 (-160)	-18 (-45)	1165 (1080)	126 (-158)	1280 (1455)
702	85 (62)	583 (614)	85 (-95)	-5570 (-4980)	67 (-148)	276 (268)
704	-9 (-5)	85 (-5)	-196 (-222)	-441 (-179)	2680 (2920)	912 (1030)
705	111 (98)	-18 (22)	-476 (-530)	77 (8)	1700 (1590)	-390 (-507)
711	53 (22)	-9 (-9)	4800 (4920)	27 (110)	2050 (2060)	254 (382)
717	76 (125)	-27 (-178)	1975 (2070)	205 (384)	94 (86)	-169 (-63)
712	9 (76)	125 (360)	555 (432)	294 (-720)	-49 (28)	136 (104)

[a]Values from inertial loads.

[b]Values from strain gages.

Table 19. Summary of high-level tests

Mode	High-level mode	High-level frequency Hz	Ratio[a]	Control-ling member	Load, N (lb)	Stress, $N/m^2 \times 10^4$ (psi)	Damping $\rho = \dfrac{c}{c_{cr}}$
708	708	4.51	4.48	751	557 (125)	278 (430)	0.020
743	753	4.65	5.98	754	417 (93.6)	207 (321)	0.020
701	701	7.84	1.07	754	2320 (520)	1145 (1780)	0.007
702	732	8.29	1.56	752	1600 (360)	844 (1309)	0.006
704	704	11.43	1.51	755	1650 (370)	825 (1280)	0.005
705	705	13.95	1.41	752	1770 (398)	744 (1150)	0.004
711	711	15.32	1.39	664	1280 (287)	1190 (1848)	0.007
709	709c	19.61	7.10	750	352 (79)	1610 (250)	0.010
712	712	19.47	1.84	750	1350 (304)	629 (975)	0.013
707	747	24.39	2.42	A-P47	-	1335 (2065)	0.014
713	713	26.39	1.31	753	1910 (428)	845 (1311)	0.007
714	714	29.44	3.12	754	800 (180)	405 (629)	0.009

[a]Ratio of $\dfrac{\text{specified limit}}{\text{actual load}}$

Fig. 1. Modal test configuration

Fig. 2. Node identification
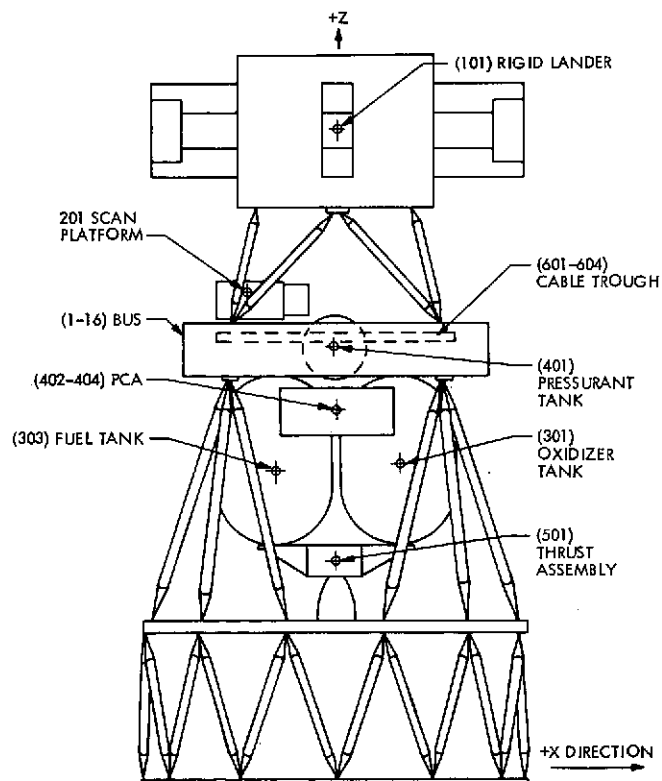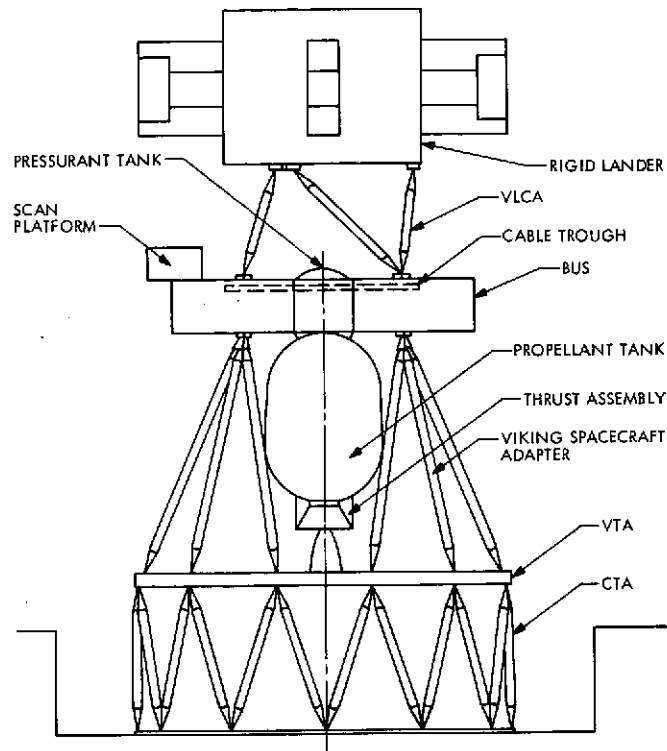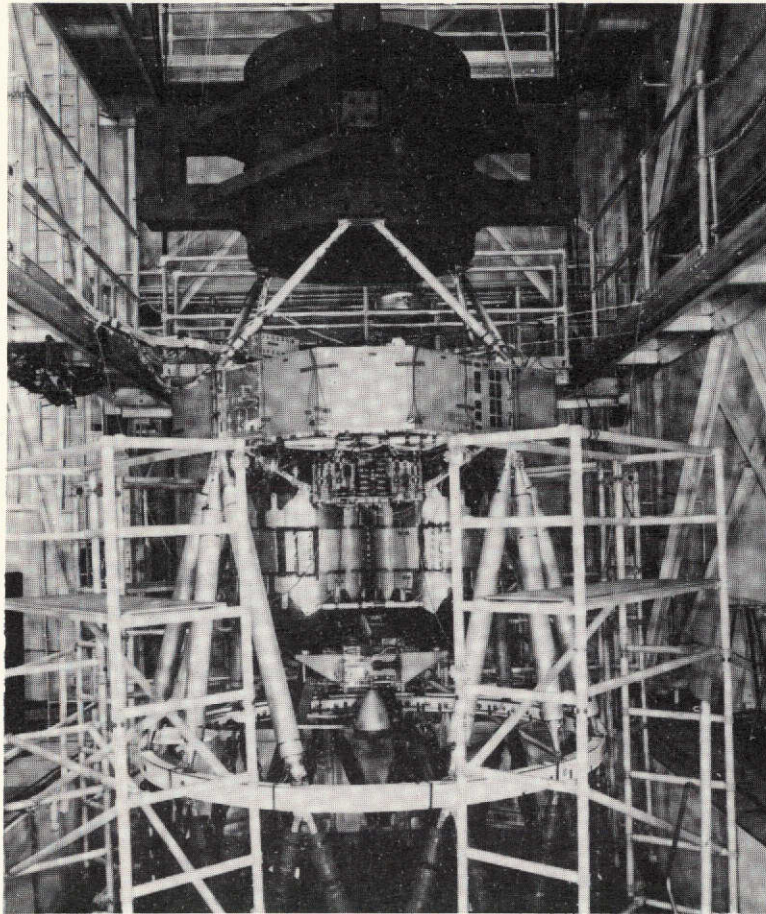
Fig. 3a. Modal test setup
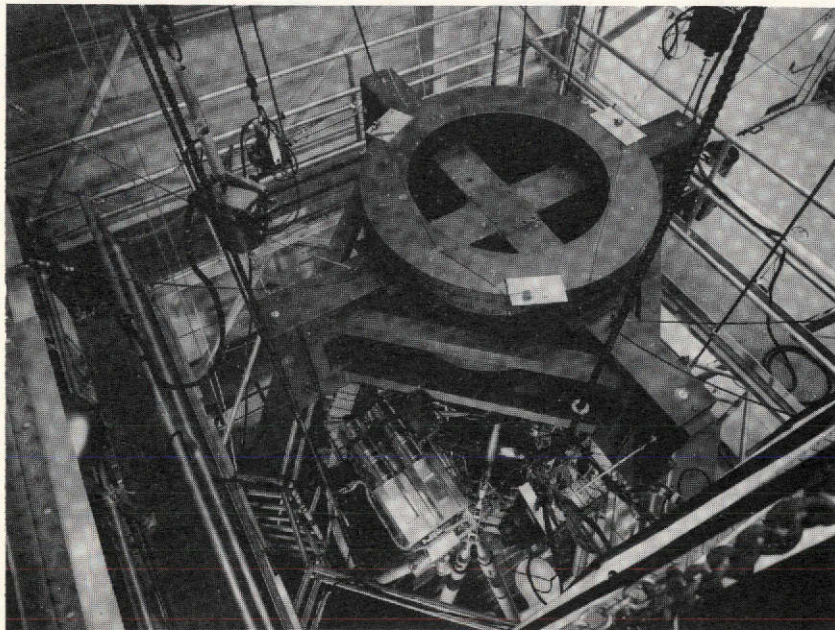
Fig. 3b. Modal test setup, vertical view
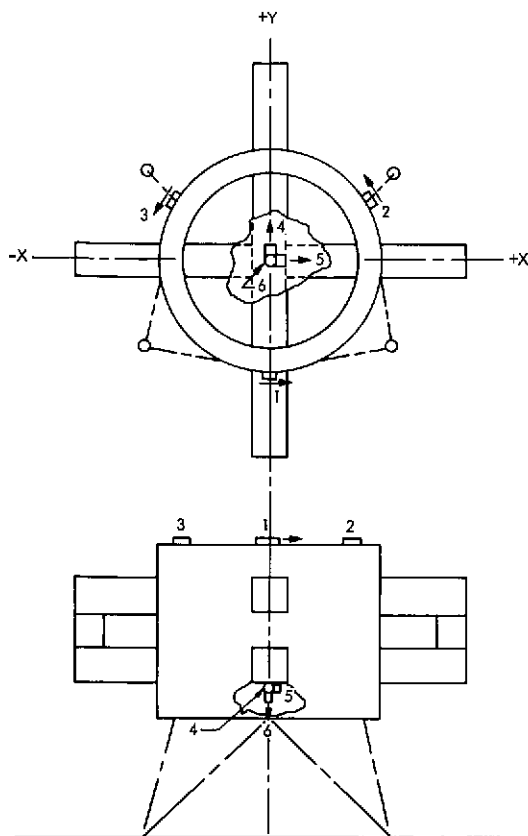
Fig. 4a. Accelerometer positions, rigid lander
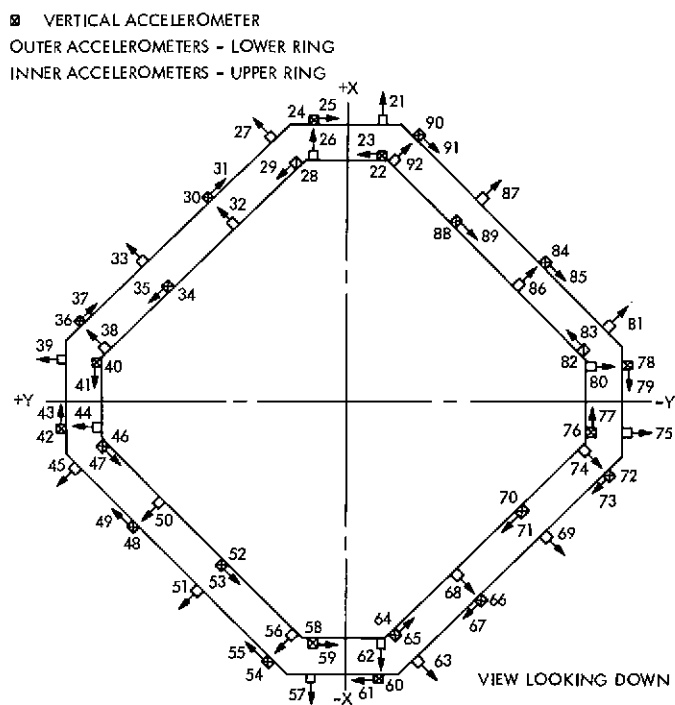
Fig. 4b. Accelerometer positions, bus
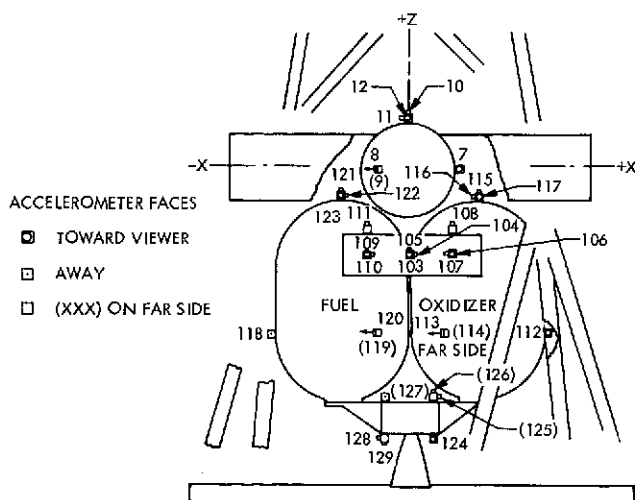
Fig. 4c. Accelerometer positions, propulsion subsystem
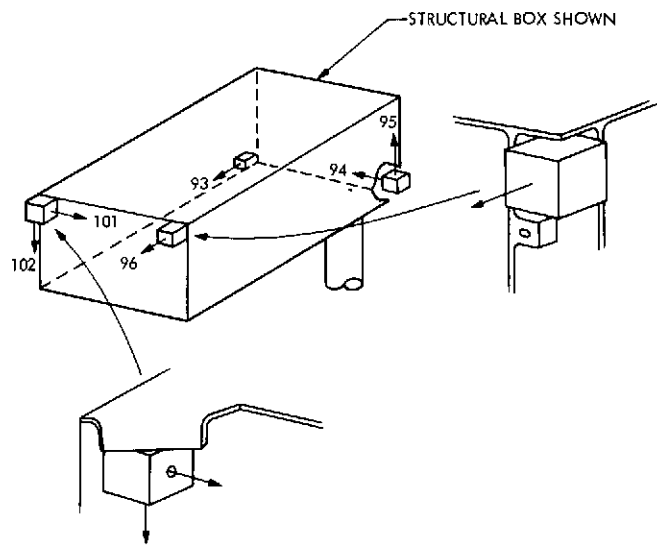
Fig. 4d. Accelerometer positions,
scan platform
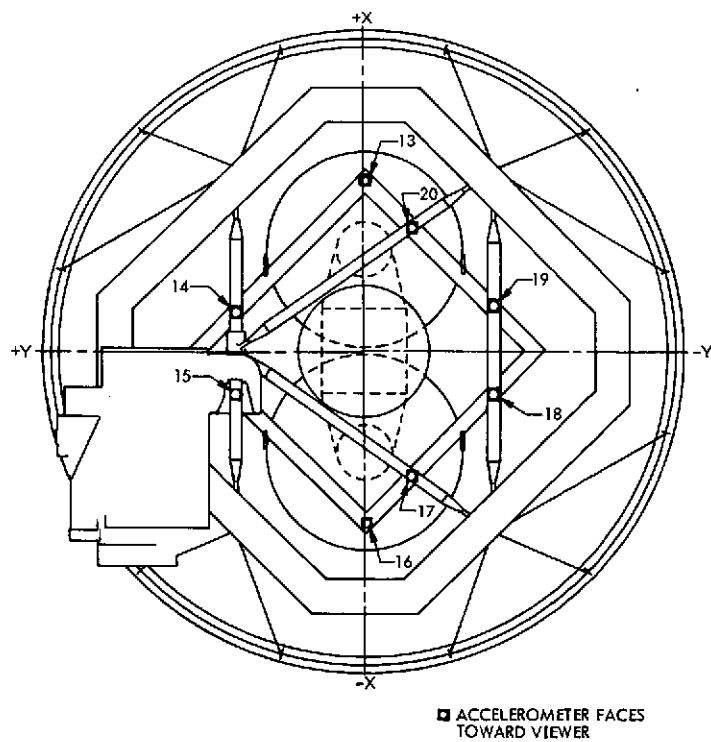
Fig. 4e. Accelerometer positions,
cable trough
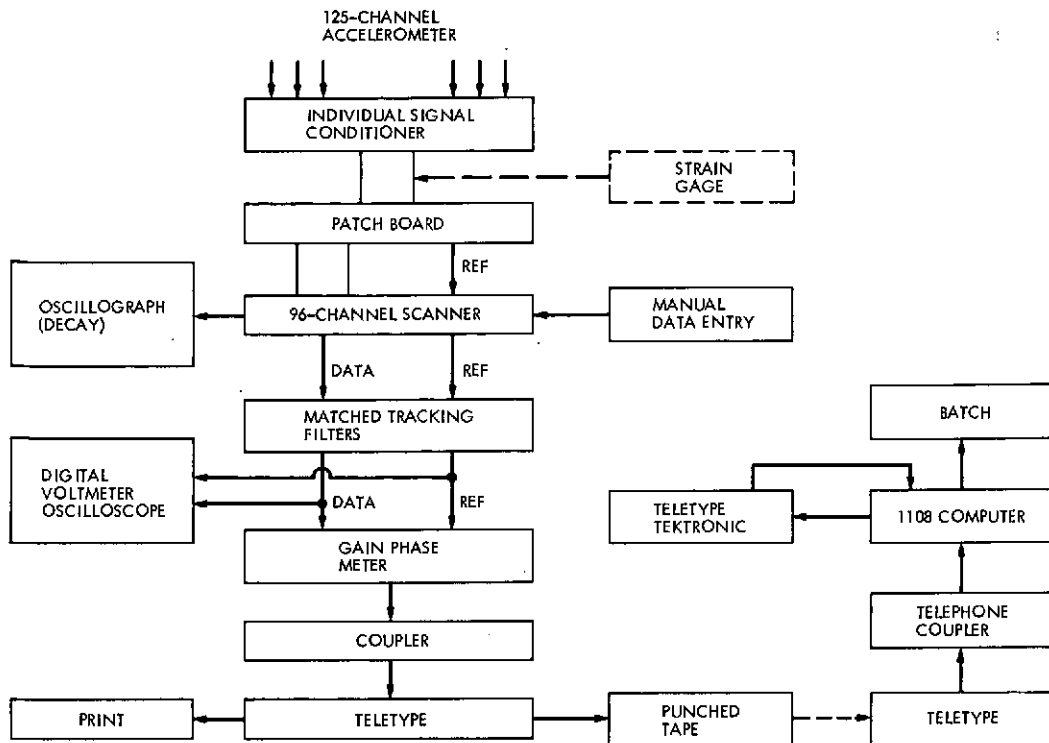
Fig. 5a. Accelerometer data acquisition
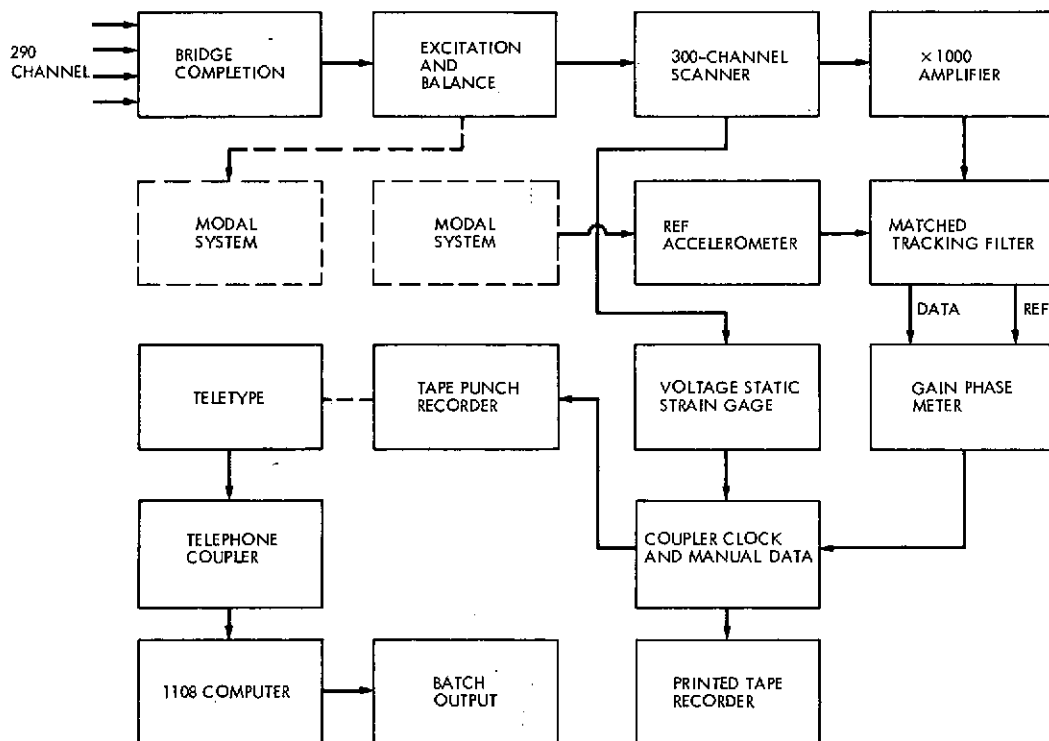
Fig. 5b. Strain gage data acquisition
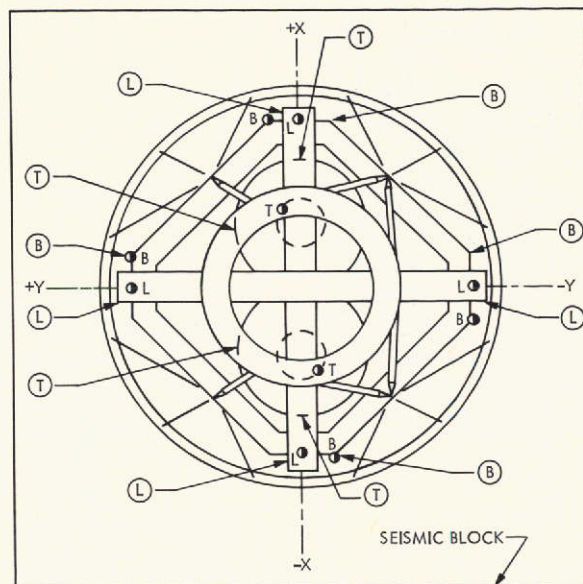
EXCITATION POINTS

LATERAL	VERTICAL		POSITION
Ⓛ	L ◖		LANDER
Ⓑ	B ◖		BUS
Ⓣ	T ◖		PROPELLANT TANK
	POSITION AS INDICATED		

Fig. 6a. Shaker positions
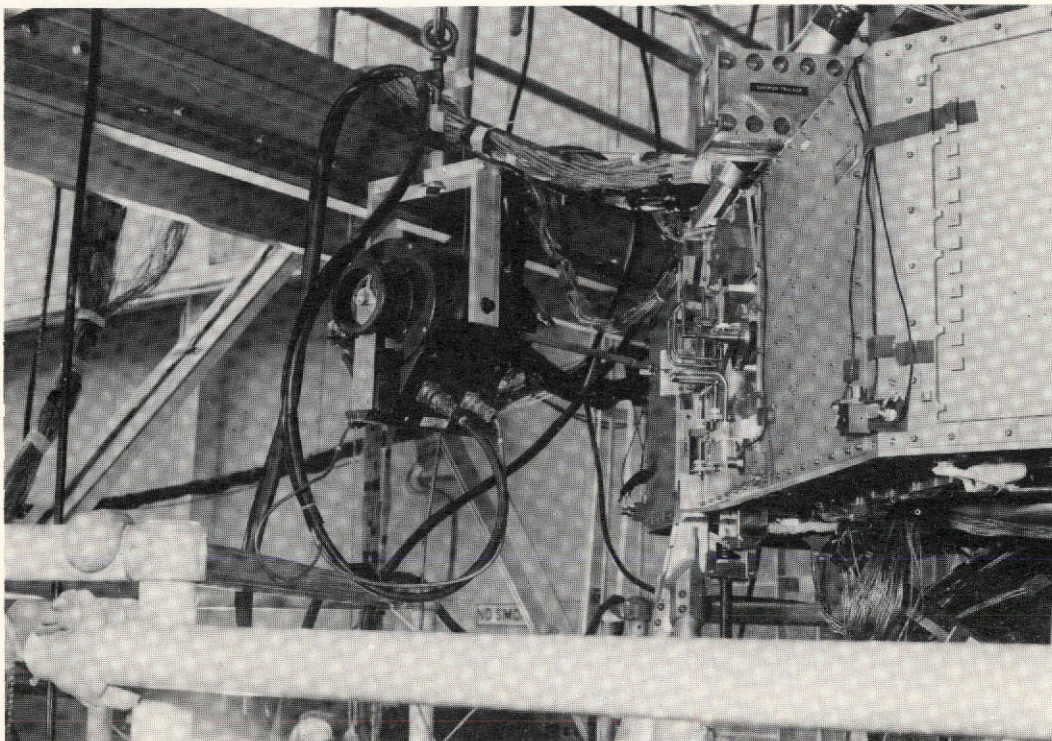
Fig. 6b. Shaker attachment to bus
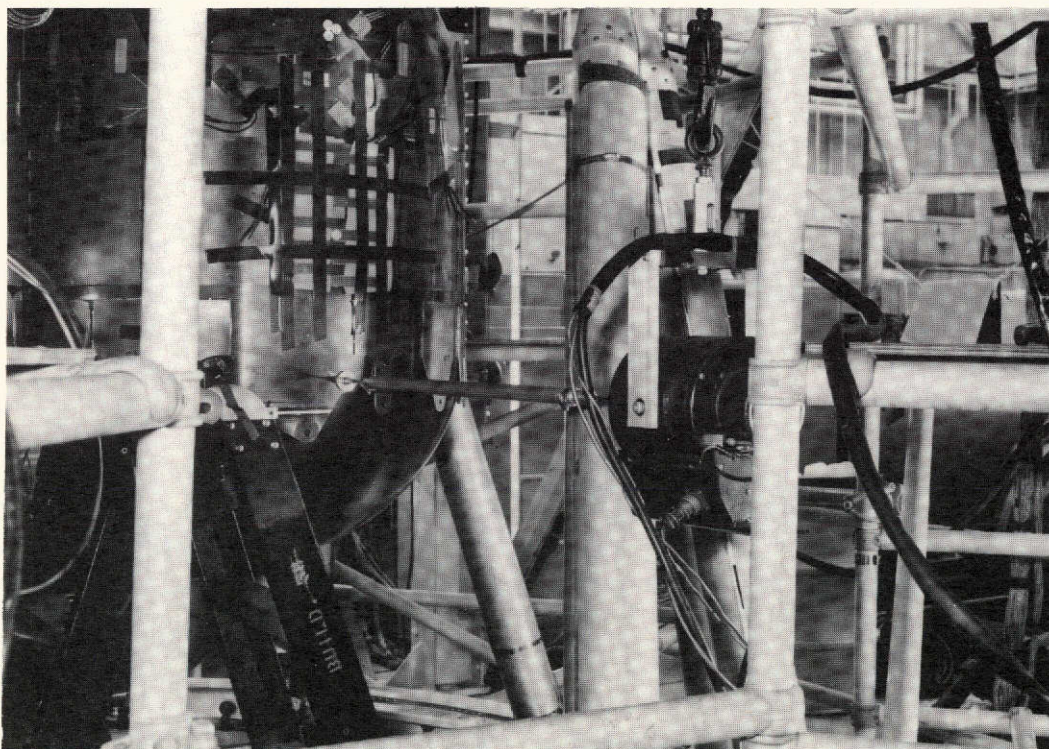
Fig. 6c. Shaker attachment to propellant tank
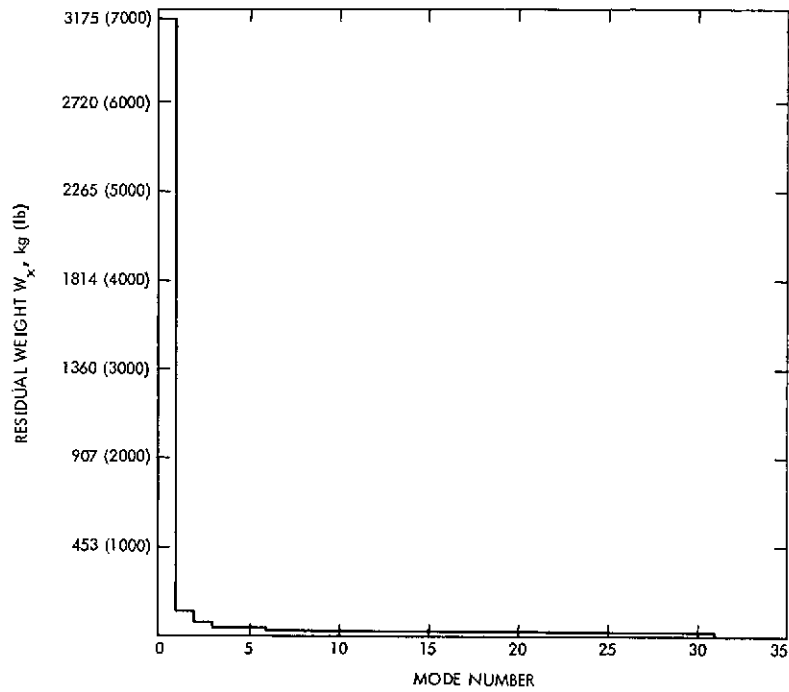
Fig. 7a. Analytical residual
weight plot, W_x
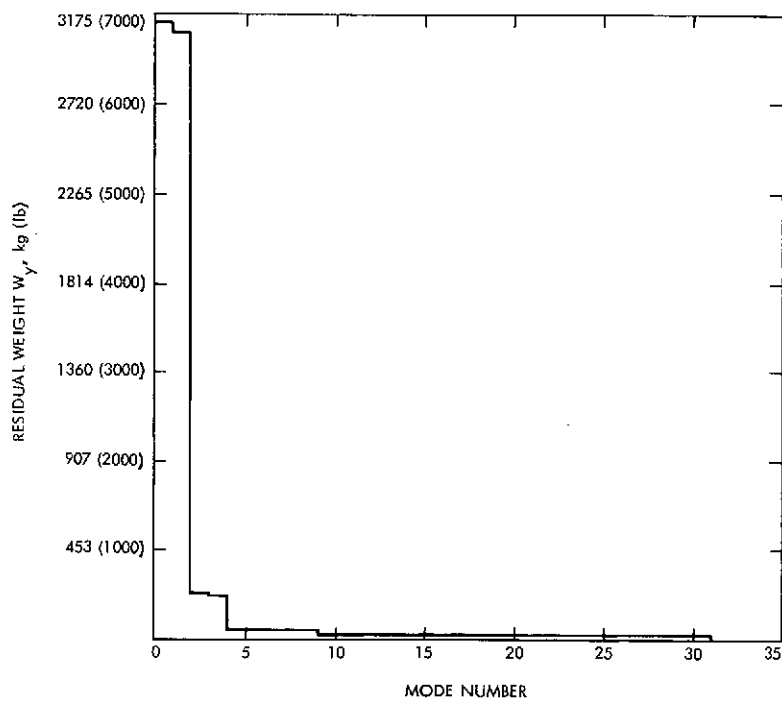
Fig. 7b. Analytical residual
weight plot, W_y
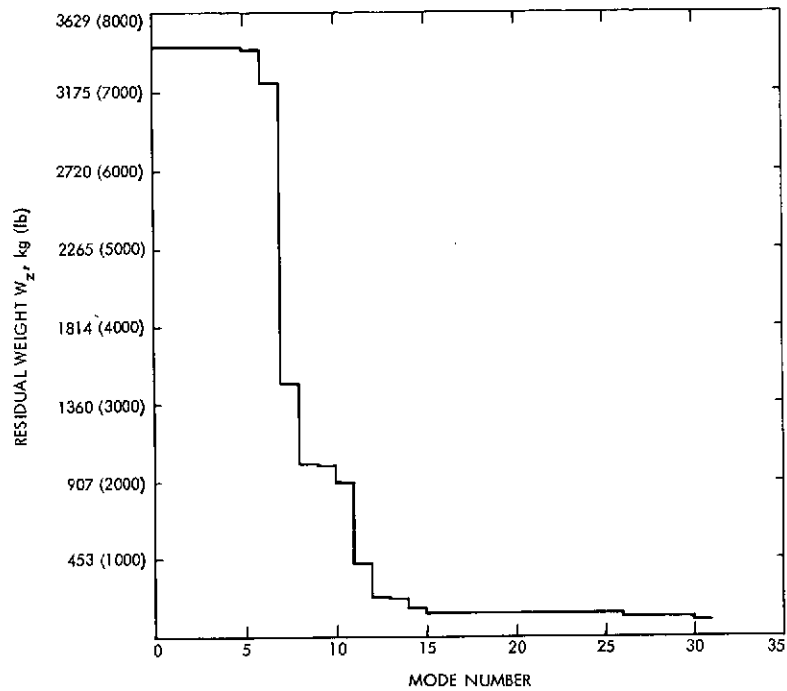
Fig. 7c. Analytical residual
weight plot, W_z
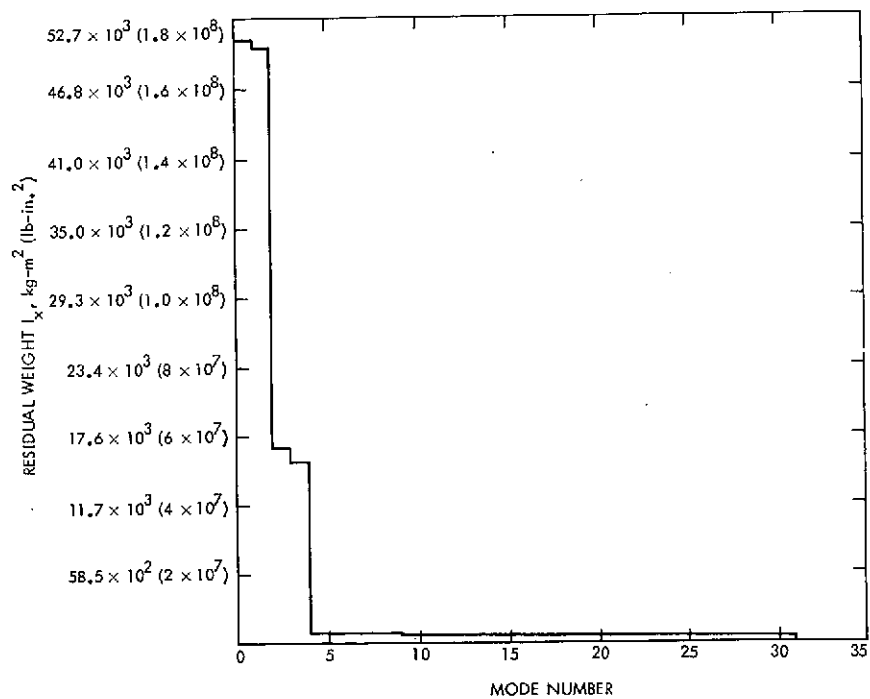
Fig. 7d. Analytical residual weight
plot, I_x
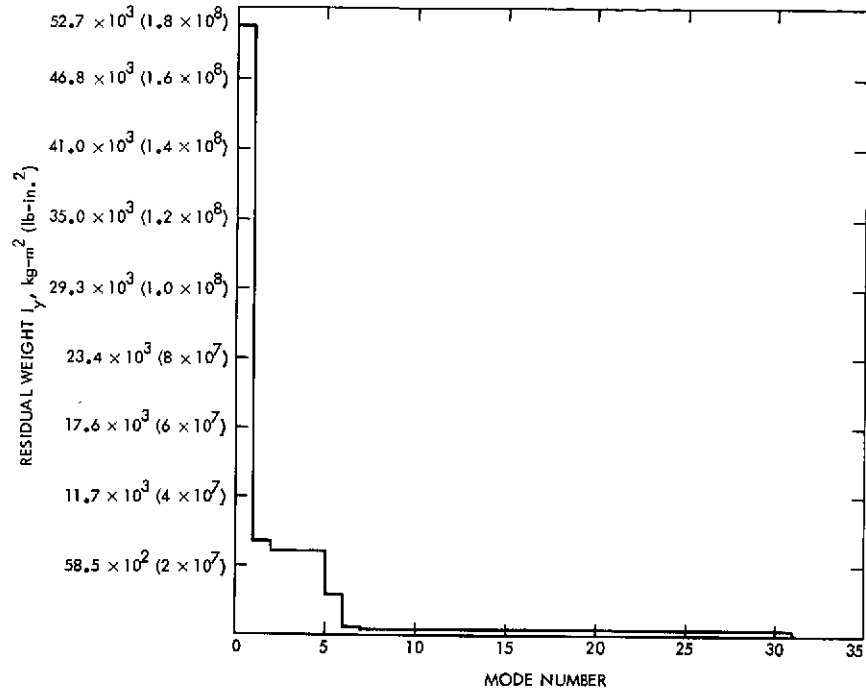
Fig. 7e. Analytical residual weight
plot, I_y
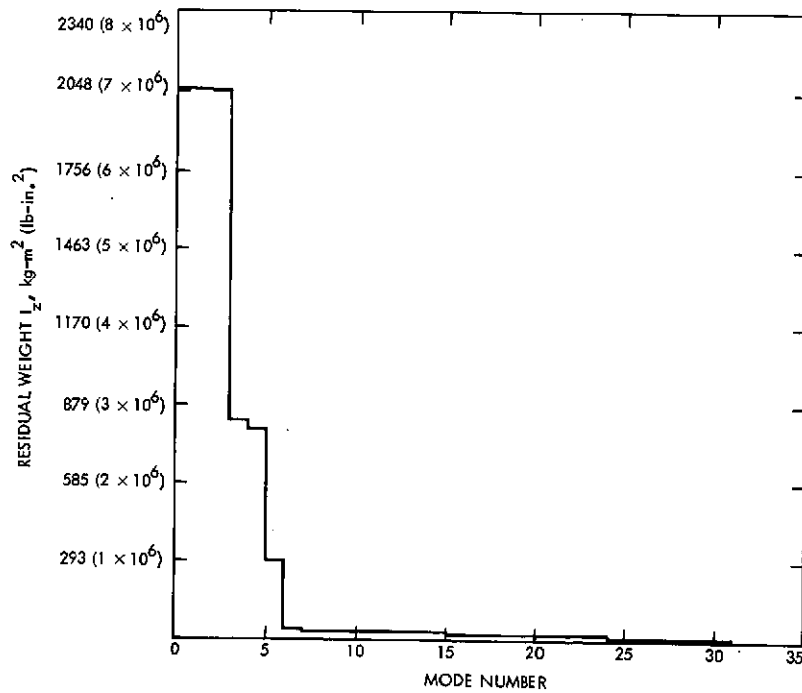
Fig. 7f. Analytical residual weight
plot, I_z

X-COORDINATE AXIS DIRECTION (ANALYSIS)
DASHED LINES INDICATED MODAL DISPLACEMENT
ANALYSIS MODE 3, FREQUENCY 7.48 Hz
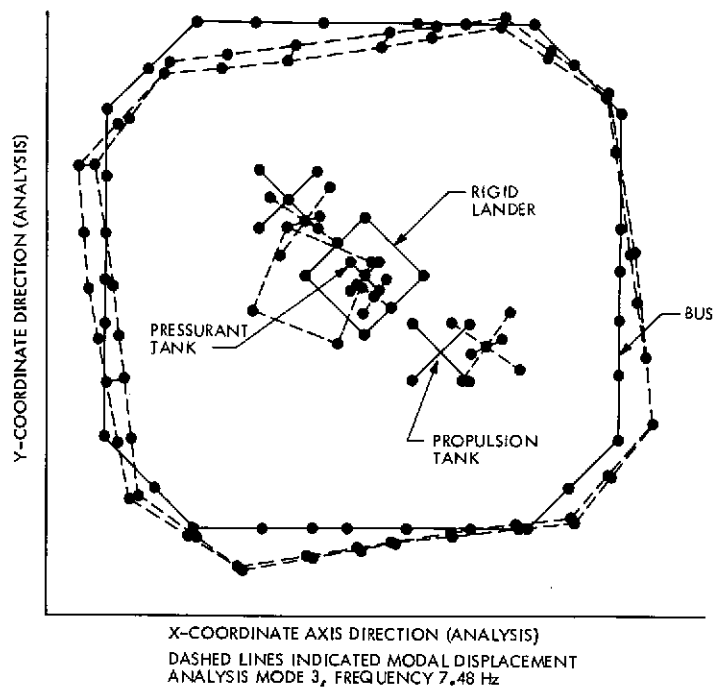
Fig. 8a. Analytical mode shape,
projection in x-y plane

Y-COORDINATE AXIS DIRECTION (ANALYSIS)
DASHED LINES INDICATE MODAL DISPLACEMENT
ANALYSIS MODE 3, FREQUENCY 7.48 Hz
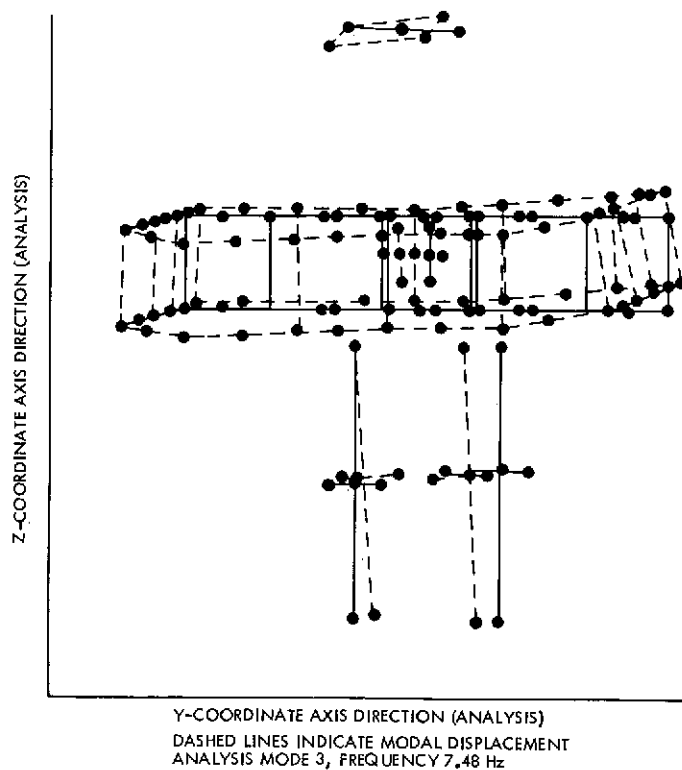
Fig. 8b. Analytical mode shape,
projection in y-z plane

X-COORDINATE AXIS DIRECTION (ANALYSIS)
DASHED LINES INDICATE MODAL DISPLACEMENT
ANALYSIS MODE 3, FREQUENCY 7.48 Hz
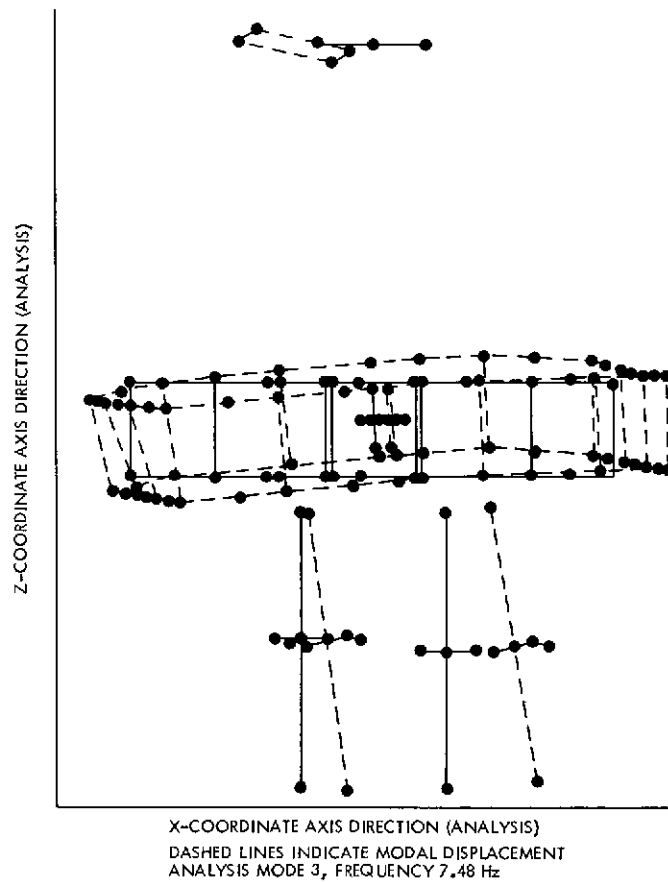
Fig. 8c. Analytical mode shape,
projection in x-z plane
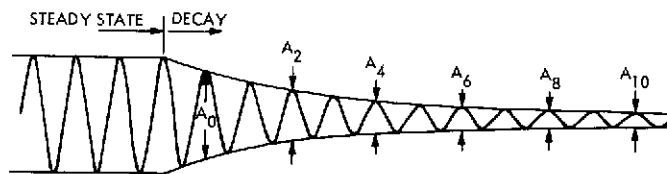
$$2\frac{c}{c_{crit}} = \frac{1}{\pi(K-J)}\ln\left(\frac{A_K}{A_J}\right)$$

WHERE A_K IS AMPLITUDE AT K_{th} PEAK

             A_J IS AMPLITUDE AT J_{th} PEAK

             $(K-J)$ IS NUMBER OF CYCLES BETWEEN

EXAMPLE: $2\frac{c}{c_{crit}} = \frac{1}{\pi(4)}\ln\left(\frac{A_6}{A_2}\right)$

             $K = 6$
             $J = 2$
             $(K-J) = 4$

Fig. 9. Damping decay measurements

X-COORDINATE AXIS DIRECTION (ANALYSIS)
DASHED LINES INDICATE MODAL DISPLACEMENT
TEST MODE 701, FREQUENCY 7.84 Hz
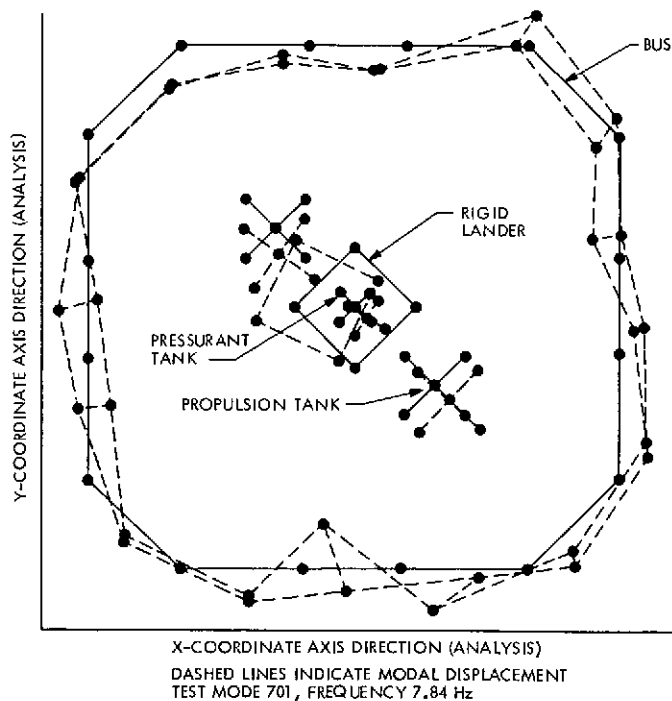
Fig. 10. Distorted experimental
mode shape

Y-COORDINATE AXIS DIRECTION (ANALYSIS)

X-COORDINATE AXIS DIRECTION (ANALYSIS)
DASHED LINES INDICATE MODAL DISPLACEMENT
TEST MODE 701, FREQUENCY 7.84 Hz
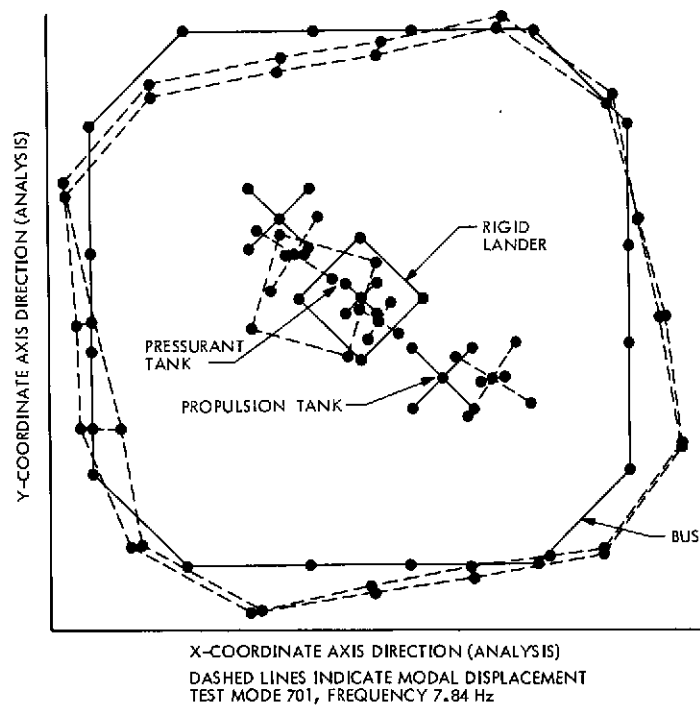
Fig. 11. Valid experimental
mode shape
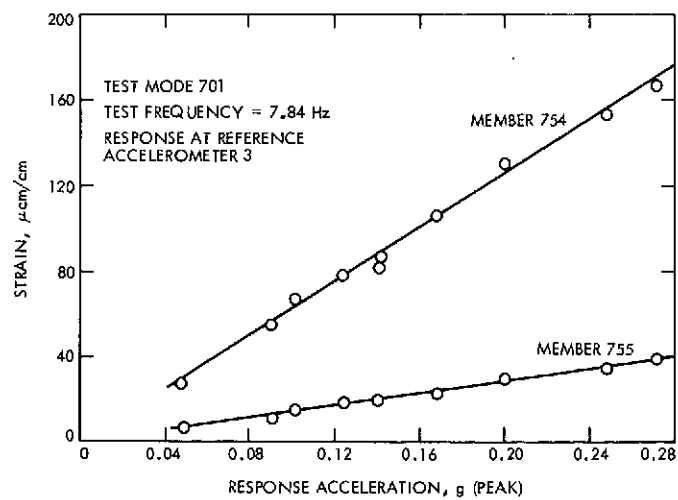
Fig. 12. Strain vs response acceleration
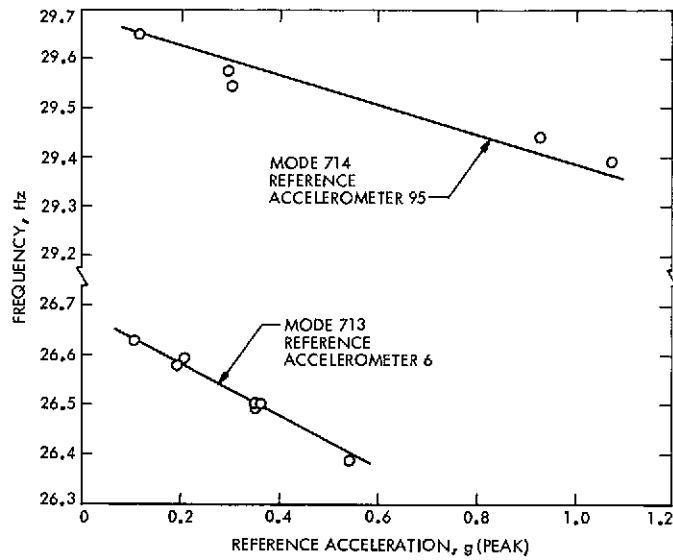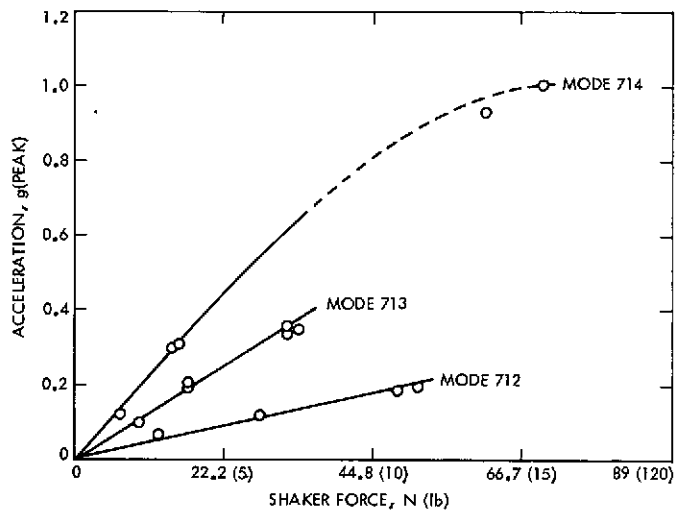
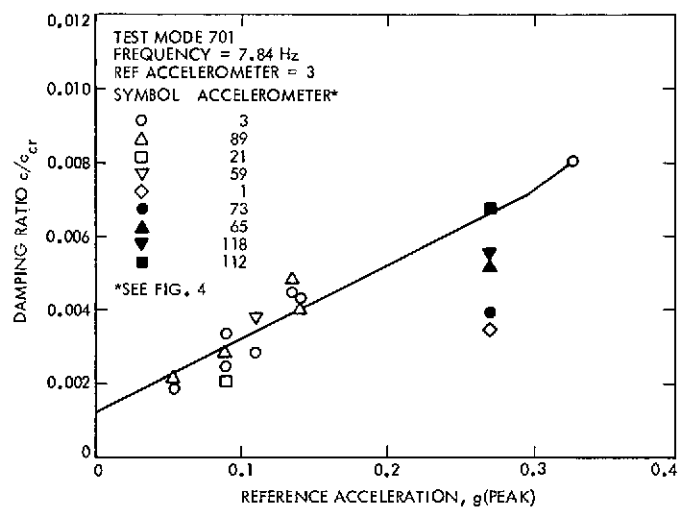Fig. 13.   Linearity frequency vs response

Fig. 14.   Acceleration vs shaker force

Fig. 15. Linearity damping vs response

APPENDIX

STRUCTURAL REPRESENTATION FOR MODAL PLOTS

Modal plots can supply important information for selecting shaker positions and phasing and for recognition of the identity of measured modes, providing that simple but adequate representation of the structure is possible. Even with simple representation, the overlapping of the neutral position of the structure by the dynamic displacement shape can be confusing.

Figures A-1 and A-2 are top and side views of the structural representation used for the ODTM tests. The propellant tanks and the pressurant tanks are represented by three orthogonal lines to define translation in three directions and rotation about three axes. The lander is described with a flat plate and the continuous bus structure by a series of points along the outer edge at the top and bottom of the bus structure.

Heavy dots define positions from which the computer calculates modal displacements for the analytic solutions or for experimental measurements. The neutral position is delineated by solid lines connecting the dots; the dynamic displacement is shown by dashed lines.
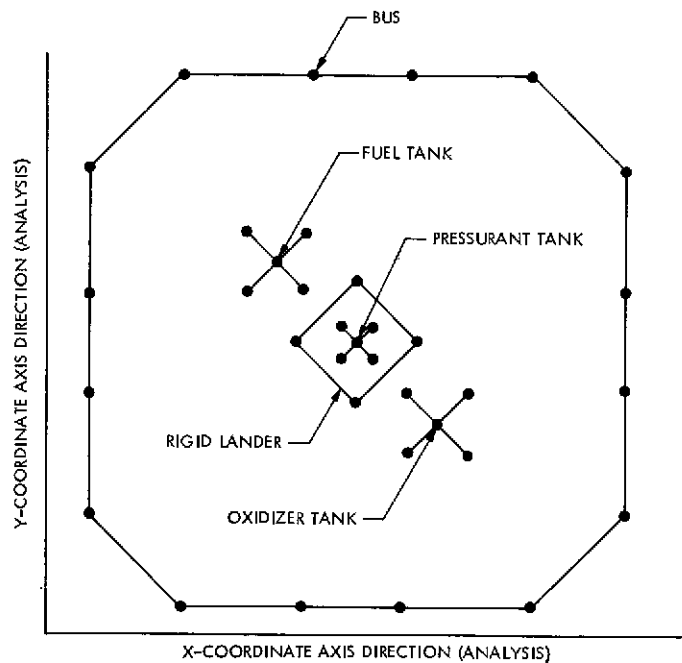
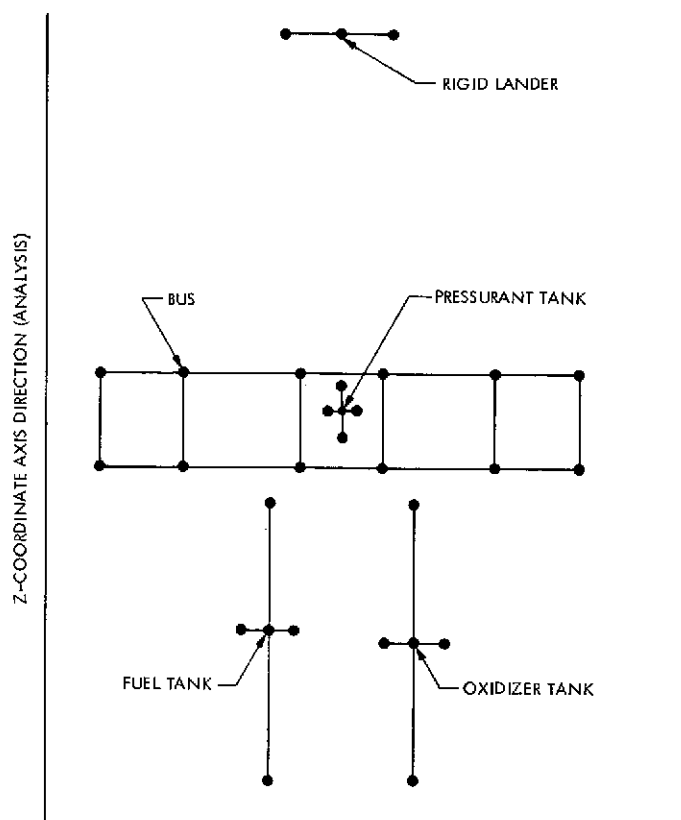Fig. A-1. Structure representations for
modal plots, top view

Fig. A-2. Structure representations for
modal plots, side view